CONFERENCE PRE-PRINT

NEW INSIGHTS ON THE QUASICOHERENT MODE IN EDA HIGH CONFINEMENT DISCHARGES

G. Grenfell¹, T. Görler¹, J. Kalis¹, L. Gil², M. Dunne¹, P. Manz³, J. Adamek⁴, G. Birkenmeier^{1,5}, D. Brida¹, J. Cavalier⁴, G.D. Conway¹, M. Faitsch¹ M. Griener¹, T. Happel¹, T. Nishizawa⁶, M. Spolaore⁷, C. Silva² U. Stroth^{1,5}, B. Vanovac⁸, E. Wolfrum¹, and the ASDEX Upgrade team^a, and the EUROfusion Tokamak Exploitation Team^b

Email: gustavo.grenfell@ipp.mpg.de

Abstract

Intrinsic ELM-free regimes that effectively combine a high-performance fusion core with a robust power exhaust solution are pursued for a fusion reactor. The enhanced D-Alpha (EDA) H-mode is a promising ELM-free regime that fulfills several requirements for ITER and a DEMO reactor, such as low impurity content, high normalized energy confinement, compatibility with a highly radiative edge and divertor region, and high Greenwald density fraction. Nevertheless, the instability that triggers the quasicoherent mode (QCM), an edge oscillation that prevents the pressure gradient from exceeding the peeling-ballooning limit, is poorly understood, making the extrapolation of the regime to future devices uncertain. In this contribution, several turbulence fingerprints associated with the QCM are measured and compared to linear gyrokinetic simulations. The result indicates that the QCM is driven by a marginally unstable kinetic ballooning mode (KBM) in the pedestal foot.

1. INTRODUCTION

Mitigation and suppression of type-I edge-localized modes (ELMs) are key for ITER and a DEMO reactor to avoid any potential damage to their plasma-facing components during operation [1, 2]. Furthermore, those devices must operate in a regime that integrates a high-performance fusion core and a robust power exhaust solution capable of minimizing power heat loads on the divertors and first wall, as well as gross erosion. However, fulfilling all these requirements simultaneously is not a straightforward task. Intrinsic ELM-free regimes are promising solutions, each with different advantages and disadvantages when extrapolated to future devices [3]. However, as an active research topic, the scenario is constantly evolving, with the pros and cons of each regime always under debate. Among these regimes, the enhanced D-Alpha (EDA) H-mode fulfills several of those requirements [4, 6, 5], such as high normalized energy confinement, low impurity content, high Greenwald density fraction, and compatibility with a highly radiative edge and divertor region. The regime is stable and stationary, with the absence of large transient events, thanks to an edge oscillation called the quasicoherent mode (QCM) that enhances radial transport in the pedestal region [7, 8, 9], preventing the pressure gradient from overcoming the peeling ballooning boundary.

¹Max-Planck-Institut für Plasmaphysik, Boltzmannstr. 2, Garching, Germany

²Instituto de Plasmas e Fusao Nuclear, Instituto Superior Técnico, Universidade de Lisboa, 1049-001 Lisboa, Portugal

³Institute of Physics, University of Greifswald, Felix-Hausdorff-Str. 6, 17489 Greifswald, Germany

⁴Institute of Plasma Physics of the Czech Academy of Sciences U Slovanky 2525/1a 182 00

⁵Technical University of Munich, TUM School of Natural Sciences, Physics Department, 85748 Garching, Germany

⁶Research Institute for Applied Mechanics, Kyushu University, Japan

⁷Consorzio RFX (CNR, ENEA, INFN, Università di Padova, Acciaierie Venete S.p.A.), Padova, Italy

⁸Massachusetts Institute of Technology, Plasma Science and Fusion Center, Cambridge, MA 02139, USA

^aSee Zohm et al 2024 (https://doi.org/10.1088/1741-4326/ad249d) for the ASDEX Upgrade Team.

^bSee Joffrin et al 2024 (https://doi.org/10.1088/1741-4326/ad2be4) for the EUROfusion Tokamak Exploitation Team.

The QCM is the main signature of this regime, and its understanding is key to reliably extrapolating the EDA H-mode to future devices.

Investigating the nature of QCM in EDA H-mode has been an active topic. The QCM was initially proposed to be a resistive ballooning X-point mode in Alcator C-Mod [10]. Further investigations on the same device revealed that the mode enhances magnetic fluctuations [11], is only observed on the low-field side [12], and exhibits a drift-wave character for transport [8]. In addition, when detected close to the separatrix, the QCM propagates in the electron diamagnetic direction (EDD) in the co-moving (plasma) frame, but in the ion diamagnetic direction (IDD) further inside when measured with gas puff imaging (GPI) and gas puff charge exchange recombination spectroscopy (GP-CXRS) [13]. While these discrepant observations may be partially due to differences in the regime (e.g., heating, gas fueling), they may also indicate a change in the QCM character along the radius. In fact, measurements with a reciprocating ball-pen probe head at the outer midplane of ASDEX Upgrade revealed that the QCM cross-phase between density and potential fluctuations changes radially [9]. Similarly as observed in Alcator C-Mod, the mode phase velocity in the plasma frame might depend on where it is measured [9, 14]. As the kinetic profiles in the plasma edge are steep, quantities such as the plasma beta and electron collisionality can vary radially, which in turn can affect and change the characteristics of the microinstabilities, as it will be discussed. In this contribution, the reciprocating probe and the thermal helium beam diagnostic are combined to investigate the properties of the QCM in ASDEX Upgrade. Several turbulent fingerprints of the mode were measured and compared with gyrokinetic simulations in the confined region to identify potential QCM drivers.

2. LOW POWER EDA-MODE

A stationary low-power EDA H-mode was developed in ASDEX Upgrade [9] in order to maximize the number of experimental observables to compare with simulations. The experiment was carried out in lower single null favourable configuration with toroidal magnetic field of ≈ -2.5 T on-axis and plasma current ≈ 0.6 MA.

Since the EDA H-mode is favoured by high plasma shaping, in these discharges the average triangularity was $\delta_{avg}=0.39$ and elongation $\kappa=1.63$. The plasma of deuterium was externally heated using electron cyclotron resonance heating (ECRH) at 140 GHz in the second harmonic X-mode, delivering approximately 1.0 MW of power.

2.1. MHD stability analysis

The transition to the EDA H-mode is followed by an increase of the energy confinement factor (H_{98y2}) above 1. However, despite the good confinement, type I ELMs were not detected, suggesting that the pedestal was stable against this instability. To verify how closed the peeling ballooning boundary was, MHD stability analyses with the MISHKA code were performed [15]. Fig. 1 shows the flux-surface averaged edge current density $\langle j_{tor} \rangle$ by the maximum normalized edge pres-

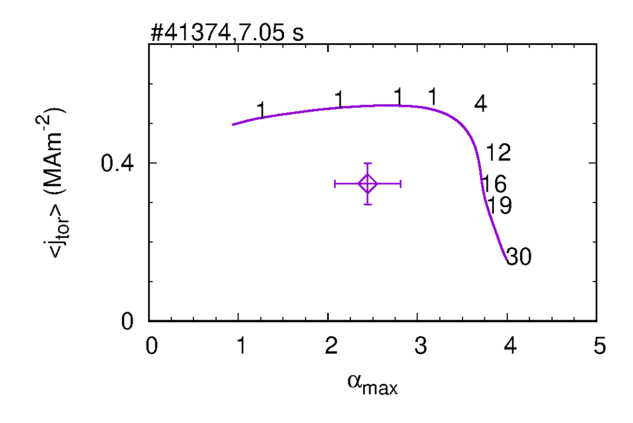


FIG. 1. Peeling-ballooning pedestal stability diagram calculated with the MISHKA code [15] for the low power EDA H-mode.

sure gradient (α_{max}) diagram. The experimental point lies in the upper right corner of the boundary, but distant (within the errorbars) from the limit.

3. EXPERIMENTAL CHARACTERIZATION OF THE QCM

The stable pedestal against the peeling-ballooning instability is associated with enhanced transport caused by the QCM [7, 8, 9], which likely clamps the pressure profile below the limit. In this section, we present and discuss the measured fingerprints of this mode.

3.1. Radial localization, mode wavenumber, and phase velocity

Fluctuations associated with the QCM are measured with a reciprocating probe equipped with ball-pen pins [16] and with the thermal helium beam (THB) diagnostics [17] at the outer midplane. Fig. 2 a) shows the mode amplitude in arbitrary units, normalized by the maximum amplitude measured by each diagnostic.

Here, the probe signal is the root-mean-square (RMS) of the ion saturation current fluctuation, which is approximately proportional to the density, while the thermal helium beam is the RMS of the emission lines ratio (667 and 587 nm) normalized by its temporal mean, which is sensitive to electron temperature and density [18]. The two diagnostics combined cover well the mode's radial extension of about 2 cm, spanning from the pedestal region into the near scrape-off layer (SOL). The maximum amplitude is just inside the separatrix. In the laboratory frame, the QCM frequency is approximately constant $f^{QCM} \approx 45 \text{ kHz across}$ its radial extension [9], even though the background $E \times B$ velocity $(v_{\theta}^{E \times B})$ varies (Fig. 2 b) in the same interval. The mode velocity ($v^{QCM} = 2\pi f^{QCM}/k_{\theta}$) is in the electron diamagnetic direction (EDD) in the lab frame. Moreover, the QCM poloidal wavenumber is found in the range $k_{\theta} \rho_s \approx 0.02 - 0.05$ (where $\rho_s = \sqrt{m_i T_e}/eB$ is the ion gyroradius) [9,14], increasing slightly towards the SOL [9]. In the comoving frame (i.e., plasma frame rotating with $v_{\theta}^{E \times B}$), the QCM velocity direction depends on the radial position. In the confined region, the mode propagates between the EDD and the IDD (within the error bars).

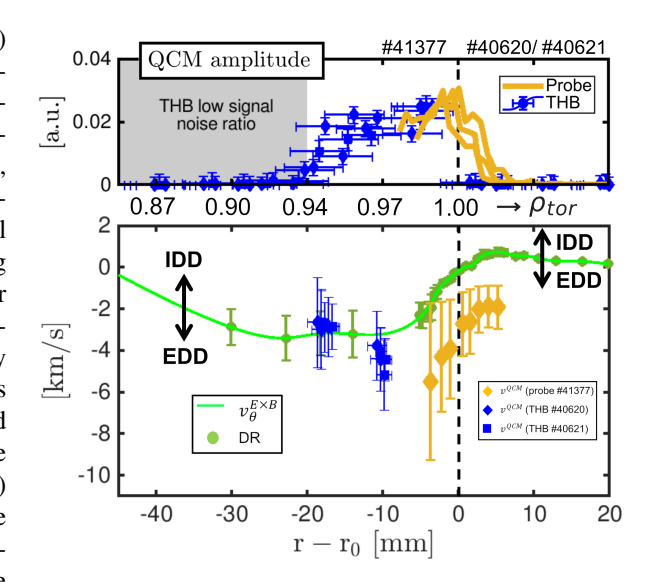


FIG. 2. QCM normalized amplitude measured with the reciprocating probe and the thermal helium beam (THB); b) background $E \times B$ velocity measured with the Doppler reflectometry (DR) is compared to the QCM phase velocity. The green line shows a spline fit on the data. $EDD/IDD = electron/ion\ diamagnetic\ direction$.

In the SOL, however, it is primarily in the EDD. Such variation in the velocity keeps the mode frequency in the laboratory frame constant, and it is connected with changes in the mode characteristic [9]. For an expanded database of EDA H-mode and QCE discharges, the QCM (as measured by THB) was estimated to propagate in the IDD at its highest amplitude [14], under the assumption that $E_r \approx \nabla p_e/(en_e)$, where p_e is the electron pressure and n_e the electron density.

3.2. Cross-phase: $n \times T_e$

The excited spectral lines of a helium gas injected into the plasma provide information on the electron temperature and density [17]. In order to decouple the individual contributions of these quantities, the ratio of the combined lines must be taken, which also excludes the influence of helium atom density. However, the emission intensity of some of these lines is often weak, making them more susceptible to noise. If the noises are uncorrelated (e.g., photon noise), the linearized spectrum correlation technique allows minimizing their impact [19]. Furthermore, by selecting an appropriate combination of lines, for which the ratio is sensitive primarily to either n_e or T_e , while maximizing the signal with respect to photon noise, and applying the linearized spectrum correlation technique between nearby channels, the cross-phase between density and electron temperature (α_{nT_e}) can be computed.

On this purpose, we select channels 7 and 19, as both are located in the confined region just inside the separatrix (see Fig. 3 a), where the QCM exists and has a large amplitude. Fig. 3 b) shows the normalized cross-power spectrum between density and electron temperature, the square cross-coherence, and α_{nT_e} . The QCM is clearly visible in the first two signals (gray shaded area) with low cross-phase, around zero. Note that due to the higher coherence of the QCM, above the background noise level (red dashed line), the error of α_{nT_e} is the lowest within its spanned frequency.

3.3. Cross-phase: $n \times \phi$

The reciprocating ball-pen probe allows us to measure several plasma quantities with high spatial and temporal resolution. In particular, by combining probe tips that measure ion saturation current and the ball-pen potential, in a balanced way to reduce phase errors, one can infer the turbulent radial particle flux [16]. In fact, this diagnostic enabled us to quantify transport caused solely by the QCM [9]. An interesting observation, however, was that the cross-phase between density and potential fluctuations ($\alpha_{n\phi}$), which is connected with the radial particle flux $\Gamma_r \propto k_\theta \sin \alpha_{n\phi}$, varies radially within the QCM frequency range. While in the SOL/separatrix regions, the values of $\alpha_{n\phi}$ are close to zero, which is a fingerprint of drift-wave instabilities, as also observed in Alcator C-mod [8], $\alpha_{n\phi}$ gradually becomes more anti-correlated towards the confined region, i.e., between $-\pi/2$ and $-\pi$. Such a

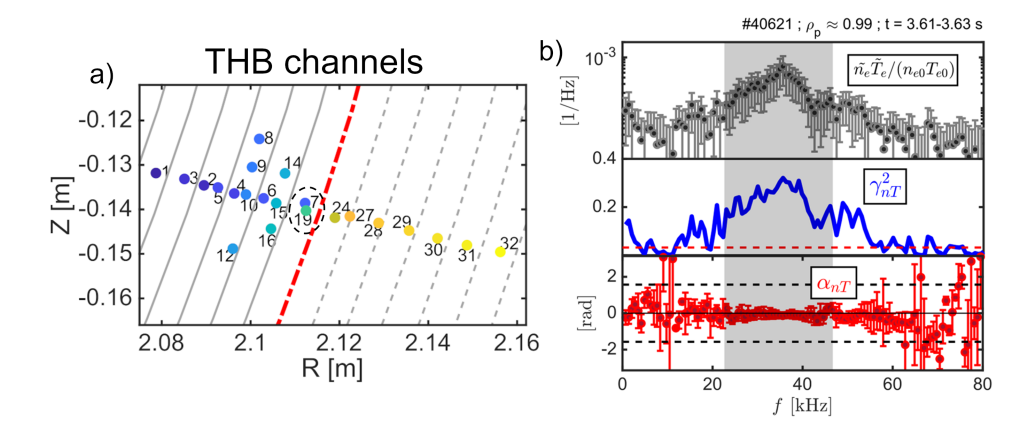


FIG. 3. a) Thermal helium beam (THB) channels for discharge #40621; b) normalized cross-power between density and electron temperature fluctuations, square of the cross-coherence, and α_{nT_e} for a low power EDA H-mode.

cross-phase is a fingerprint of electromagnetic instabilities [25], like the kinetic ballooning mode (KBM) [26, 27].

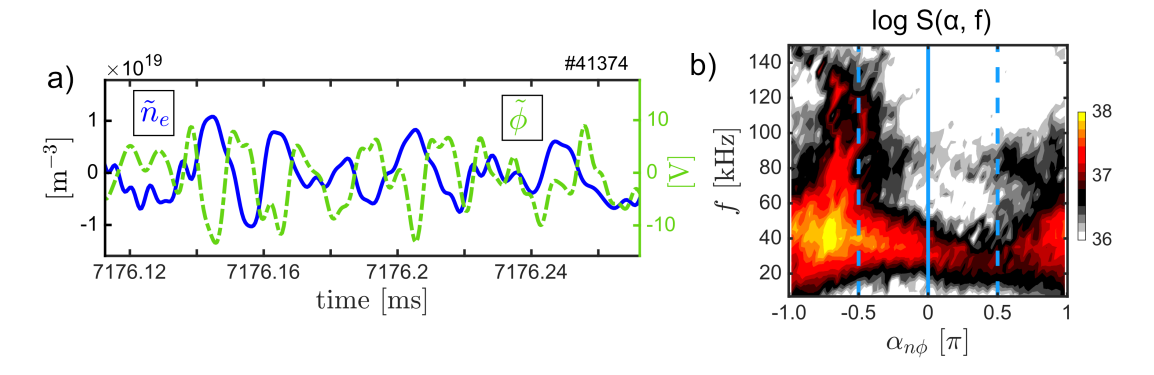


FIG. 4. a) Density and potential fluctuation measured with the reciprocating ball-pen probe [16] and b) cross-power spectrum distribution as function of the frequency and the cross-phase between density and potential fluctuations ($\alpha_{n\phi}$) at $\rho_p \approx 0.99$.

Fig. 4 a) shows the density and potential fluctuations when the probe was at $\rho_p \approx 0.99$. From the raw \tilde{n}_e and $\tilde{\phi}$ fluctuations, one can see that these quantities are most of the time anti-correlated. Focusing on the QCM frequency, which ranges from approximately 20 to 60 kHz, we see in Fig. 4 b) that this is the interval where cross-power spectrum distribution $S(\alpha,f)$ has the highest amplitude, while $\alpha_{n\phi}$ is between $-\pi$ and $-\pi/2$. Note that the minus sign here is due to how the cross-phase is defined, and does not necessarily indicate inward transport, as the flux also depends on the sign of k_{θ} . In fact, the QCM induces radially outward particle flux, as has been published elsewhere [9]. It should also be noted that the low cross-phase between density and electron temperature at the QCM frequency (Fig. 3) reduces to the minimum any influence of the electron temperature fluctuations on the potential measured by the ball-pen probe [16].

4. LINEAR GYROKINETIC SIMULATION

In order to establish a quick orientation concerning the microinstabilities in the pedestal region of the low-power EDA H-mode and identify potential QCM drivers, we performed local (flux-tube) linear gyrokinetic simulations with the electromagnetic, Eulerian, delta-f Vlasov code GENE [20, 21] in the absence of the equilibrium $E \times B$ shear.

Fig. 5 shows the input profiles for the simulations. Here, the density was measured with Thomson scattering, Li-beam, and the midplane reciprocating probe, the electron temperature with Thomson scattering and the reciprocating probe, and the ion temperature with CXRS and the reciprocating probe from the swept ball-pen probe

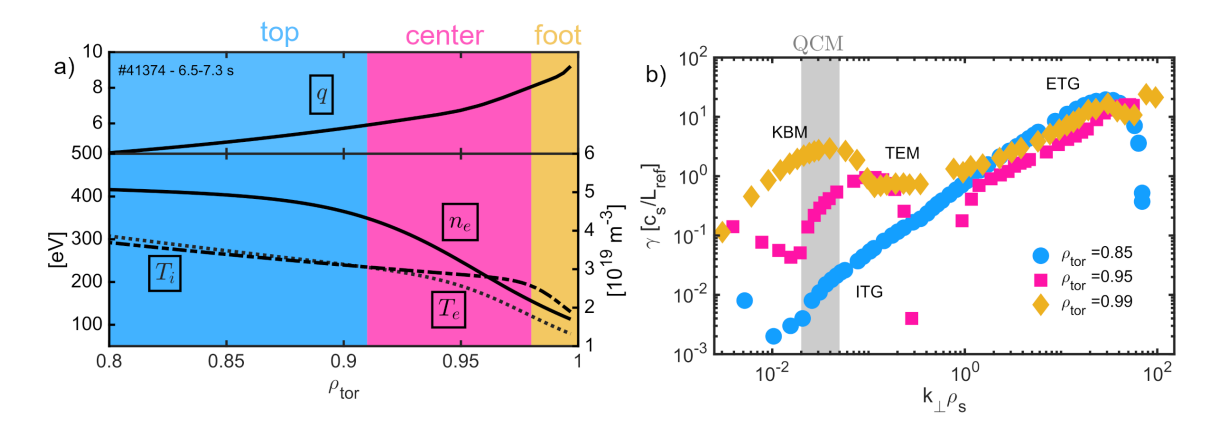


FIG. 5. a) Input profiles for the gyrokinetic simulations: safety factor, electron density and temperature, and ion temperature. b) Maximum growth rate over the ballooning angles for three different ρ_{tor} in the pedestal top, center, and foot as a function of the normalized perpendicular wavenumber $k_{\perp}\rho_{s}$. The shaded gray area shows the experimental $k_{\perp}\rho_{s}$ range that the QCM is observed.

technique [22]. All profiles were mapped to the equilibrium reconstruction from integrated data analysis [23] and fitted with a modified hyperbolic tangent function [24].

To facilitate the discussion and comparison with the experiment, the pedestal was divided into three regions: top, center, and foot (Fig. 5 a). In each region, a set of microinstabilities was identified. Fig. 5 b) shows the maximum growth rate for three different ρ_{tor} , with the electron scale results being maximized over ballooning angle. At the pedestal top, we observe that the electron and ion temperature gradient modes (ETG and ITG) are the dominant microinstabilities. Moving to the pedestal center, ETG is still present in the electron scale, while the dominant instability in the ion scale becomes the trapped electron modes (TEM). Finally, at the pedestal foot, TEM still exists in the ion scale, but the highest growth rate is for a KBM at lower $k_{\perp}\rho_{s}$. ETG is also seen in the pedestal foot, being, therefore, present in the whole pedestal. The impact of the impurity was also assessed by adding boron as a third species based on its measured density profile. The results show a qualitatively similar physical picture, but with slightly reduced growth rates.

5. COMPARISON WITH THE EXPERIMENT

As a first comparison, by overplotting the QCM experimental $k_{\perp}\rho_s$ range in Fig. 5 b), we see that ITG, TEM, and KBM are within the same interval, therefore are potential candidates for the QCM drive instability. However, as shown in Fig. 1, the QCM highest amplitude is somewhere between the pedestal foot and center, thus ITG can be discarded. Based on the growth rate, the KBM has the highest amplitude at the QCM wavenumber, while the TEM peaks at the pedestal center for a higher $k_{\perp}\rho_s$. Moreover, KBM modes propagate in the ion diamagnetic direction in the co-moving (plasma) frame, whereas TEM modes propagate in the electron diamagnetic direction. As can be seen in Fig. 2 b), the QCM phase velocity appears to vary with radius. While this result may be related to changes in the mode character [9], the large error bars of the mode phase velocity when mapped to the co-moving frame make it difficult to draw any firm conclusions. In addition to the uncertainties in the alignment of the probes and THB channels and their finite sizes, the mode frequency is broad in the lab frame, while the radial electric field has significant error bars.

Focusing on the pedestal foot and center, we compare the simulations with the experimental turbulence cross-phases

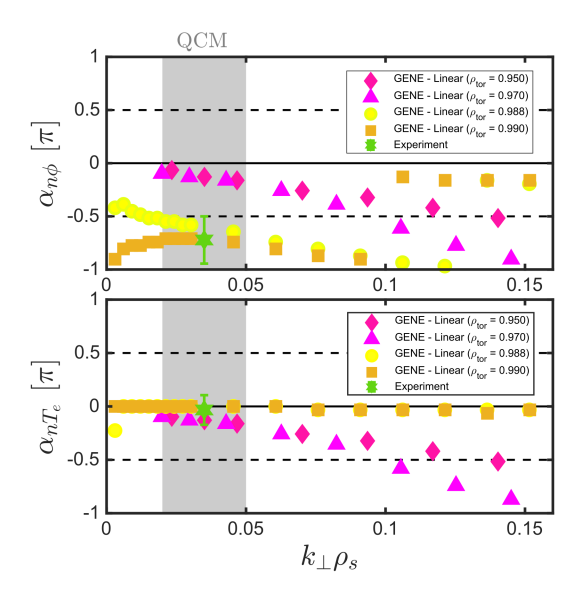


FIG. 6. Comparison between GENE linear simulations and experiment (at $\rho_{tor} \approx 0.985 - 0.995$) at two locations at the pedestal foot where the KBM is dominant instability and two at the pedestal center where TEM is dominant.

between density and electron temperature (α_{nT_e}) , measured with the THB diagnostic (Fig. 3), as well as between the

plasma potential and density $(\alpha_{n\phi})$, measured with the probe (Fig. 4). Fig. 6 shows that the experiment is in line with the simulation results within the QCM perpendicular wavenumber range (gray area) in the pedestal foot, where the KBM is the dominant microinstability. The electron temperature and density fluctuations are in phase, whereas density and potential fluctuations are closer to $-\pi$. In the pedestal center, where TEM is the dominant instability, both $\alpha_{n\phi}$ and α_{nT_e} are close to zero. Therefore, based on the set of turbulent fingerprints observed experimentally and compared with the simulations, the KBM emerges as the main candidate for the QCM drive instability.

5.1. Sensitivity scan in β

The simulations presented in the previous sections are gradient-driven, i.e., the background profiles are fixed. Nevertheless, given the inherent uncertainties associated with diagnostics and plasma fluctuations, this approximation might not be realistic. To assess the sensibility of the results presented in the previous sections, we have performed a plasma β scan focused on the pedestal foot at $\rho_{tor}=0.99$ and toroidal mode number n=13 corresponding to the maximum KBM growth rate in Fig 5 b). In GENE, β can be changed independently on other parameters, which is ideal to decouple its effect.

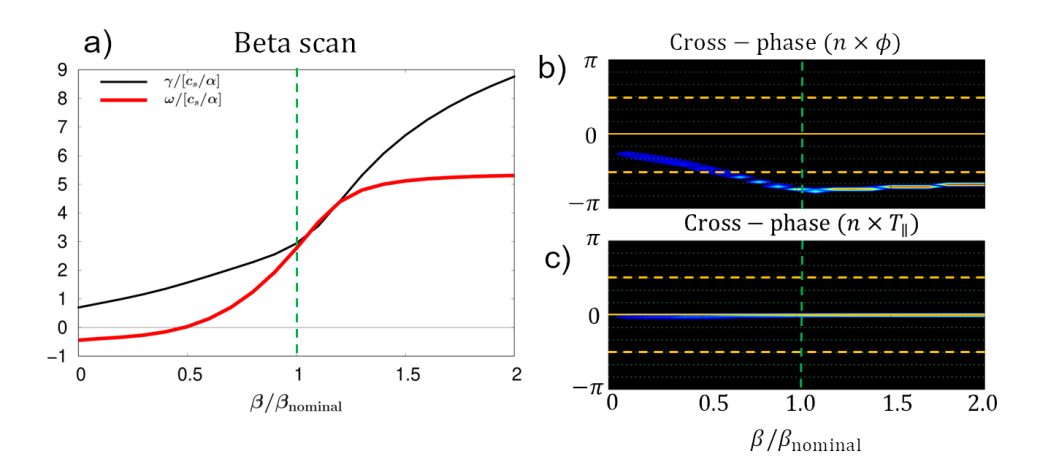


FIG. 7. GENE linear simulation: β scan at $\rho_{tor}=0.99$ and fixed toroidal mode number n=13. a) Growth rate (γ) and frequency (ω) ; b) cross phases between density and potential, and density and electron temperature (parallel component).

Fig. 7 a) shows how the mode growth rate (γ) and frequency (ω) change with the β normalized by the nominal value. The rapid increase of γ with beta is a further characteristic of KBM [26]. Likewise, ω increases around the nominal β and then saturates for higher values. Reducing β results in a smaller reduction of γ , while ω drops more substantially, flipping sign for $\beta/\beta_{\text{nominal}} \approx 0.5$ (i.e., propagates in the EDD). The mode at this point is no longer a KBM, but rather a type of electrostatic drift wave.

Fig. 7 b) shows how $\alpha_{n\phi}$ varies with β . At the nominal value, $\alpha_{n\phi}$ is between $-\pi$ and $-\pi/2$, which is a fingerprint of a KBM, as discussed in the previous section. For higher β , $\alpha_{n\phi}$ shifts slightly towards $-\pi/2$, which is a more favorable cross-phase for transport: the KBM becomes more unstable. On the other hand, decreasing the beta from its nominal value leads to a gradual shift of $\alpha_{n\phi}$ to zero. For $\beta/\beta_{\text{nominal}} < 0.5$, ω is negative, while $\alpha_{n\phi}$ lies between $-\pi/2$ and 0. The mode changes its character, becoming an electrostatic drift wave/interchange instability. Interestingly, the cross-phase between density and electron temperature $\alpha_{nT_{\parallel}}$ (Fig. 7 c) and $\alpha_{nT_{\perp}}$ (not shown here) are almost insensitive to the β scan.

The scan suggests that the KBM is marginally unstable. By increasing β , both γ and the radial transport increase, as $\alpha_{n\phi}$ becomes more favorable for transport (i.e., closer to $-\pi/2$). If the profiles were allowed to vary (e.g., in flux-driven simulations), that would reduce β and, consequently, the growth rate, likely bringing the values back to the nominal one. However, if the transport is too violent, the KBM could be destabilized and replaced by an electrostatic drift wave.

5.2. Sensitivity scan in collisionality

Similarly, one can scan only the collisionality, while keeping the other parameters constant with GENE. In addition, electromagnetic effects can be switched off by running an electrostatic version of the code. Fig. 8 a) shows the growth rate (γ) as a function of the electron collisionality (ν) normalized by the nominal value. Reducing ν by a factor of 10 only slightly changes the growth rate in both electromagnetic (nominal) and electrostatic simulations. Conversely, rising ν leads to an almost $x^{1/3}$ increase of γ for the electromagnetic case, while for the electrostatic, the rise is faster initially until it converges to the electromagnetic one at higher ν values. Such a behavior is reminiscent of the electrostatic resistive ballooning mode (RBM) scale reported elsewhere [28].

At the nominal ν , the mode is a KBM and the cross-phase between density and potential (Fig. 7 b) lies between $-\pi$ and $-\pi/2$. As ν decreases, $\alpha_{n\phi}$ shifts to $-\pi$, which makes the mode potentially more stable as the cross-phase becomes more unfavorable for transport. Increasing ν , $\alpha_{n\phi}$ gradually shifts towards $-\pi/2$, which make it more unstable. The KBM becomes more RBM-like. Similarly to the β scan, $\alpha_{nT_{\parallel}}$ barely changes with the collisionality.

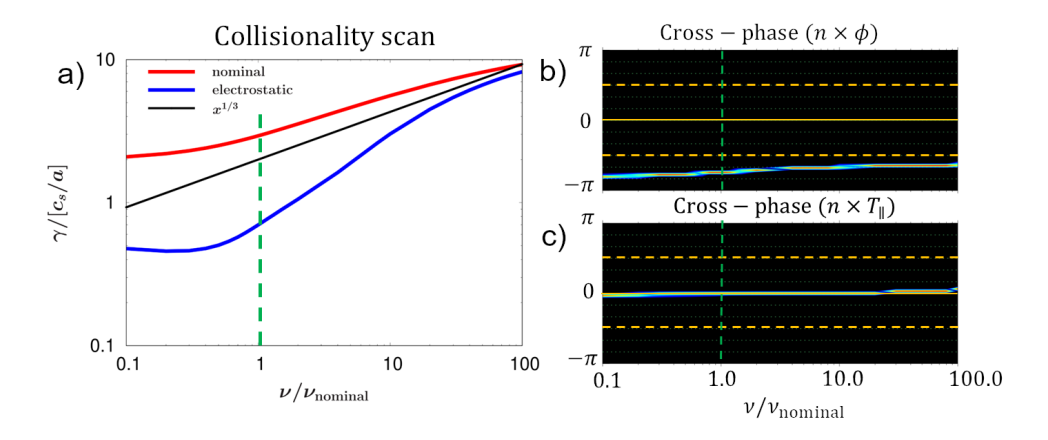


FIG. 8. Linear GENE collisionality (ν) scan at $\rho_{tor}=0.99$ and toroidal mode number n=13: a) Growth rate (γ); b) cross phases between density and potential, and density and electron temperature (parallel component).

6. GLOBAL LINEAR SIMULATIONS

In a local simulation, the modes are confined to the flux tube and profiles are considered to be constant along the simulation domain. However, in a more realistic scenario, the different excited modes should have a radial extension that may overlap when considered together globally and with the profile variation. This behavior is captured in global gyrokinetic simulations [21]. To verify the consistency of the local linear simulations previously presented, we have performed linear-global simulations with GENE, i.e., the modes are now allowed to grow beyond the narrow flux tubes but the modes don't yet interact, which is a feature of non-linear simulations. The first step was to check the global behaviour without a radial electric field, i.e., without $E \times B$ shear stabilization. Interestingly, the dominant mode at toroidal mode number n=13 corresponding to the growth rate maximum in the local scan did not reproduce the cross phases matching the experimental measurements. It is still an electromagnetic mode, however, with electron diamagnetic drift direction. The previously observed KBM at the pedestal foot (in the local linear runs) can only be recovered at n=13 with β variation outside the uncertainties. At lower mode numbers around n=5, however, a mode localized between $\rho_{\rm tor}=0.97-0.999$ can be observed matching the KBM features discussed above. This mode also remains when applying the external $E \times B$ shear. All in all, this provides confidence regarding the mode identification. Future work will need to address the question to which degree this mode is affected by nonlinear interaction. Also, it should be recalled that GENE is a field-aligned code and therefore limited by the separatrix. A second task left for codes not bound by this limit (e.g., GENE-X) will be to assess the impact of neglecting the QCM's SOL fraction on the turbulence and transport inside the separatrix.

7. CONCLUSION

A comparison of the QCM experimental fingerprints with linear gyrokinetic simulations with the code GENE suggests that a marginally unstable KBM in the pedestal foot drives the QCM in the EDA H-mode in ASDEX

Upgrade. Good agreement was observed in terms of the radial location of the mode, perpendicular wavenumber, cross-phase between density and electron temperature fluctuations, and between density and potential fluctuations. Somewhat poorer agreement was seen when comparing the mode velocity in the co-moving frame. The experimental data suggest that the QCM propagates in the electron diamagnetic direction in the pedestal foot, whereas the KBM propagates in the ion direction. However, due to significant uncertainties, it is challenging to reach any definitive conclusions based solely on this information. The consistency of the local simulation was also tested in global linear simulations with GENE including the nominal background $E \times B$. The results showed a KBM between $\rho_{\rm tor}=0.97-0.999$, i.e., within the experimental QCM range. The mode also exhibits cross-phases similar to those observed experimentally, but with mode numbers around n=5, which is lower than the n=13shown by the local runs. Therefore, the global linear simulations also point to the KBM as the main candidate for the QCM drive.

Although linear simulations help us identify fingerprints that can be easily compared with experimental observations, there is no guarantee that the observed modes and their linear character would be present in global non-linear simulations. Nevertheless, the good agreement observed with several linear features of a KBM is impressive and suggests that the linear character of the mode may be preserved to some extent. Non-linear gyrokinetic and global flux-driven simulations are planned for the future, which will be important to check the consistency of the linear analysis and to understand pedestal-SOL coupling. The extrapolability of this result to future fusion reactors is not straightforward, but the implications of an unstable KBM in the pedestal foot of future reactors need to be better addressed, especially if the EDA H-mode (or variants of this regime) becomes the route pursued for a fusion reactor.

ACKNOWLEDGEMENTS

This work has been carried out within the framework of the EUROfusion Consortium, funded by the European Union via the Euratom Research and Training Programme (Grant Agreement No 101052200 — EUROfusion). Views and opinions expressed are however those of the author(s) only and do not necessarily reflect those of the European Union or the European Commission. Neither the European Union nor the European Commission can be held responsible for them.

REFERENCES

- [1] R. A. Pitts et al. Nuclear Materials and Energy, 20, 100696
- [2] H. Zohm et al. 2021 Fusion Eng. Des. 166 112307[3] E. Viezzer et al 2023 Nucl. Mater. Energy 34 101308
- [4] M. Greenwald et al 1999 Phys. Plasmas 6 1943–9
- [5] L. Gil et al 2025 Nucl. Fusion 65 046002
- [6] A. Kallenbach et al 2020 Nucl. Fusion 61 016002
- A.E. Hubbard et al 2001 Phys. Plasmas 8 2033-40
- [8] B. LaBombard et al. 2014 Phys. Plasmas 21, 056108
- [9] G. Grenfell et al 2024 Nucl. Fusion 64 104002
- [10] A. Mazurenko et al. 2002 Phys. Rev. Lett. 89 225004
- [11] J.A. Snipes et al. 2001 Plasma Phys. Control. Fusion 43 L23
- [12] J.L. Terry et al 2005 Nucl. Fusion 45 1321
- [13] C. Theiler et al. 2017 Plasma Phys. Control. Fusion 59 025016
- [14] J. Kalis et al 2023 Nucl. Fusion 64 016038
- [15] A. Mikhailovskii et al. 1997 Plasma Phys. Rep.[16] G. Grenfell et al. 2022 Rev. Sci. Instrum. 93 023507
- [17] M. Griener et al. 2018 Rev. Sci. Instrum. 89, 10D102
- [18] G. Grenfell et al. 2025 Nucl. Fusion 65 086023
- [19] T. Nishizawa et al. 2021 Rev. Sci. Instrum. 92, 103501
- [20] F. Jenko et al. 2000 Phys. Plasmas 7 1904
- [21] T. Görler et al. 2011 Journal of Computational Physics, 230(18), 7053-7071
- [22] J. Adamek et al 2021 Nucl. Fusion 61 036023
- [23] R. Fischer et al. 2016 Fusion Sci. Technol. 69 526–36
- [24] R.J. Groebner et al 2001 Nucl. Fusion 41 1789
- [25] B. Scott B 2021 Book, Volume 1
- [26] H. Doerk et al. 2016 Plasma Phys. Control. Fusion 58 115005
- [27] W. Zholobenko et al. 2024 Nucl. Fusion 64 106066
- [28] C. Bourdelle et al. 2012 Plasma Phys. Control. Fusion 54 115003
- [29] K. Stimmel et al. 2022 Journal of Plasma Physics, 88(3), 905880315.